AD-A045 120 NAVAL OCEAN SYSTEMS CENTER SAN DIEGO CALIF F/G 20/1
PARABOLIC EQUATION PREDICTIONS COMPARED WITH ACOUSTIC PROPAGATI--ETC(U)
AUG 77 K M GUTHRIE, D F GORDON

UNCLASSIFIED NOSC/TR-133 NL

1 OF 1
AD
A045120

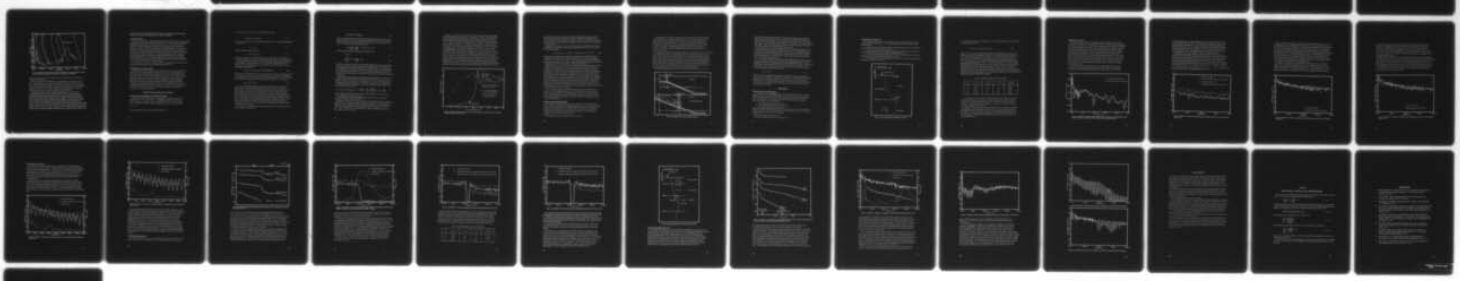

END
DATE
FILMED
11-77
DDC

NOSC

NOSC TR 133

NOSC TR 133

Technical Report 133

PARABOLIC EQUATION PREDICTIONS COMPARED WITH ACOUSTIC PROPAGATION MEASUREMENTS FROM PROJECT TASMAN TWO

KM Guthrie
Visiting Scientist from Defence Scientific Establishment,
Auckland, New Zealand
and DF Gordon

1 August 1977

Final Report: Oct 1975 – Dec 1975
Prepared for
Naval Sea Systems Command

Approved for public release; distribution unlimited

NAVAL OCEAN SYSTEMS CENTER
SAN DIEGO, CALIFORNIA 92152

NAVAL OCEAN SYSTEMS CENTER, SAN DIEGO, CA. 92152

AN ACTIVITY OF THE NAVAL MATERIAL COMMAND

RR GAVAZZI CAPT, USN
Commander

HOWARD L BLOOD, PhD
Technical Director

ADMINISTRATIVE INFORMATION

This report describes work sponsored by the Naval Sea Systems Command, Sonar Technology Office (NSEA 06H1), under Problem SF52-552-602, Task 19344. The work was performed at NUC from October to December 1975.

The Tasman Two data used in this analysis were collected by the Defence Scientific Establishment, Auckland, New Zealand, in 1975, and were provided to the US Navy under the auspices of the Mutual Weapons Defense Data Exchange Agreement, MWDDEA-N-67-NZ-6201.

Coauthor Dr. K. Michael Guthrie is a member of the staff of the New Zealand Defence Scientific Establishment, and served as Exchange Scientist to the Naval Undersea Center during the time of this analysis.

Released by
M. R. Akers, Head
System Concepts and
Analysis Division

Under Authority of
H. A. Schenck, Head
Undersea Surveillance
Department

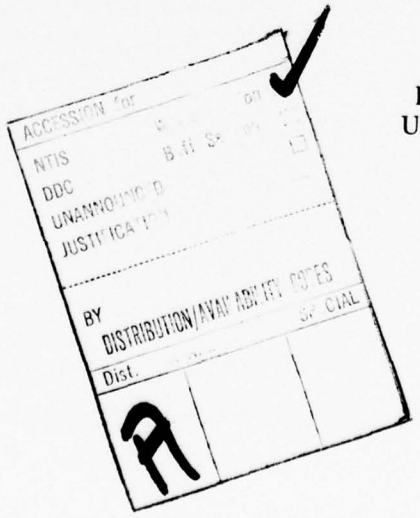

UNCLASSIFIED

SECURITY CLASSIFICATION OF THIS PAGE (When Data Entered)

REPORT DOCUMENTATION PAGE

READ INSTRUCTIONS BEFORE COMPLETING FORM

1. REPORT NUMBER: NOSC/TR-133

2. GOVT ACCESSION NO.

3. RECIPIENT'S CATALOG NUMBER

4. TITLE (and Subtitle): PARABOLIC EQUATION PREDICTIONS COMPARED WITH ACOUSTIC PROPAGATION MEASUREMENT FROM PROJECT TASMAN TWO.

5. TYPE OF REPORT & PERIOD COVERED: Final Oct 1975 to Dec 1975

6. PERFORMING ORG. REPORT NUMBER

7. AUTHOR(s): K.M. Guthrie, D.F. Gordon

8. CONTRACT OR GRANT NUMBER(s)

9. PERFORMING ORGANIZATION NAME AND ADDRESS: Naval Ocean Systems Center, San Diego, CA 92152

10. PROGRAM ELEMENT, PROJECT, TASK AREA & WORK UNIT NUMBERS: NSEA 06H1, Problem SF52-552-602, Task 19344

11. CONTROLLING OFFICE NAME AND ADDRESS: Naval Sea Systems Command, NSEA-06H1, Washington, D. C. 20362

12. REPORT DATE: 1 August 1977

13. NUMBER OF PAGES: 40

14. MONITORING AGENCY NAME & ADDRESS (if different from Controlling Office)

15. SECURITY CLASS. (of this report): Unclassified

15a. DECLASSIFICATION/DOWNGRADING SCHEDULE

16. DISTRIBUTION STATEMENT (of this Report): Approved for public release; distribution unlimited.

17. DISTRIBUTION STATEMENT (of the abstract entered in Block 20, if different from Report)

18. SUPPLEMENTARY NOTES

19. KEY WORDS (Continue on reverse side if necessary and identify by block number)

Underwater sound propagation
Acoustic propagation
Propagation loss
Parabolic equation method
South Tasman Sea

20. ABSTRACT (Continue on reverse side if necessary and identify by block number)

The parabolic equation method for computing acoustic propagation losses was used to model the results of the Tasman Two Sea Tests. In these tests aircraft dropped SUS (signals, underwater sound) charges along four great circular paths from a hydrophone near South Island, New Zealand, in westerly directions across the South Tasman Sea and Southeast Indian Ocean. The data were processed in 1/3 octave bands from 16 to 1000 Hz. The best available sound speed, bathymetric, and sediment data were compiled both from Tasman Two Sea Tests data and from historical data. These data were used to make parabolic equation runs along the radials starting at the stationary receiver for 63 and 125 Hz. Great care was required in progressing down the continental slope from the receiver and over sea mounts where small step sizes in the

→ next page

DD FORM 1 JAN 73 1473 EDITION OF 1 NOV 65 IS OBSOLETE

UNCLASSIFIED

SECURITY CLASSIFICATION OF THIS PAGE (When Data Entered)

393 159

numerical solution were required. Accurate modeling of sediments was also required in these areas. In the immediate vicinity of the hydrophone a ray theory for a wedge gave better starting values for the parabolic method than did a normal mode technique.

Agreement between computations and experiment was generally good enough to substantiate the techniques used. Poor agreement for the most southerly radial suggested inadequate knowledge of the bathymetry and sediments within 200 km of the hydrophone. Shadowing behind seamounts was found to be strongly dependent on the nature of the sediment cover.

SUMMARY

PROBLEM

Apply the parabolic equation technique to model the acoustic propagation characteristics of the south Tasman Sea and southeast Indian Ocean and compare the resulting predictions with measured acoustic data. Investigate the sensitivity of the predictions to vertical and horizontal sample step sizes and to the specification of the initial pressure distribution function. Model the acoustic shadow cast by a large bathymetric feature. Study the acoustic effects of horizontal changes in oceanography, such as the Subtropical Convergence and the Polar Front.

RESULTS

The parabolic equation technique was used to help interpret Tasman Two sea test data. Computer runs were made with realistic sound-speed and bathymetric data for ranges up to 2500 km at frequencies of 63 and 125 Hz.

A ray trace and a normal mode prediction were used to initialize the parabolic equation model in a shallow, coastal environment, but in both cases the resulting absolute levels predicted in deep water agreed with the experimental levels only to within 5 dB.

Difficulties were encountered in attempting to determine the optimum vertical sample size when running a parabolic equation prediction from shallow to deep water and vice versa.

The gross features of predicted convergence zones (width and location) as seen from the coastal site agreed well with the experimental data out to ranges of 400 km.

The predicted acoustic shadow of substantial underwater features was highly sensitive to and dependent upon the assumed properties of the sediment cover. The observed increase in shadow depth with frequency was not predicted by this model.

In certain range-dependent environments, the signal level of near-surface sources increased over ranges greater than 1000 km and the "clarity" of the convergence zone structure varied dramatically with range.

RECOMMENDATIONS

Study the use of the parabolic equation method in a wedge-shaped environment to establish criteria which can be used to determine the optimum values of vertical and horizontal sample sizes in terms of water depth, frequency, and bottom slope, with the aim of improving the accuracy of predicted signal levels.

Apply the results of this study in an attempt to predict the correct frequency dependence of the acoustic shadows formed by large underwater features.

Compare the efficiency of the parabolic equation method in a wedge with range-dependent normal mode models.

Continue this work with a quantitative investigation of the raw predicted data to see whether the variation of experimental very low frequency attenuation coefficients can be partially or wholly accounted for in terms of gross environmental characteristics (sound-speed profiles, bathymetry, sediment types).

CONTENTS

ACKNOWLEDGMENTS

We are indebted to C. D. Smith (NAVSEA, 06H1), without whose support this work would not have been possible. In addition we would like to acknowledge the efforts of Dick Bannister, Ron Denham, Dave Browning, and the technical staff at the Defence Scientific Establishment who participated in the experiment and did most of the analysis of the raw data. John Hall and DeWayne White gave us many helpful programming hints. Dick White wrote the program to generate the ray theory starters.

INTRODUCTION

In February 1975 the Ocean Science Group at New Zealand's Defence Scientific Establishment conducted a very low frequency acoustic propagation trial (Project Tasman Two) across the South Tasman Sea into the Southeast Indian Ocean (Ref. 1). The trial was a joint New Zealand, United States, Australian venture involving participation of additional personnel from the Naval Underwater Systems Center, New London, and the RAN Research Laboratory, Sydney. The aim of the experiment was to obtain an acoustic "snapshot" of the extensive oceanic region to the south-east of New Zealand and to correlate any observed changes in the acoustic propagation characteristics with known oceanographic and bathymetric features.

During October and November 1975 the authors used the parabolic equation technique (Ref. 2) to make extensive propagation loss computations along the experimental paths. The purpose of these computations was to determine the accuracy with which the experimental results could be modeled and thus determine both the effectiveness of the parabolic equation technique and the adequacy of the environmental data in describing the propagation conditions. In addition, knowledge could be gained of the propagation mechanisms revealed by the data.

The environment along each propagation path is in general strongly range dependent. The parabolic equation technique is known to work well in a deep ocean situation, where the only significant range-dependent parameter is the sound-speed profile. However, in the Tasman Two experiment certain bathymetric features are known to dominate parts of the environment. Thus the attempt to model the data represents a severe test of the parabolic equation technique.

The experience gained in this use of the parabolic equation technique and the increased knowledge of its capabilities and limitations are valuable to NOSC's acoustic prediction abilities. In addition, the acoustic properties of the ocean area included in these experiments and computations are comparatively unknown and these results are a valuable addition to the data base.

In this report the experimental procedure and environmental data are first described. Next the parabolic equation technique is introduced, with considerations of step-sizes and starting values. Finally, the particular steps of this investigation are outlined and results given. Comparisons between various computational strategies and the experimental results are shown.

EXPERIMENTAL DATA

DESCRIPTION OF TEST AREA

The hydrophone system used in Tasman Two was bottom mounted at a depth of 350 meters near 45°S 167°E (point "T") and cabled back about 6 miles to the research ship HMNZS Tui at anchor within the South Island's Thompson Sound. RNZAF aircraft flew SUS (signals, underwater sound) drops along four great circle paths, or "radials," bearing approximately NW, W, WSW, and SW from the hydrophone site. The SUS were set to detonate at 1220 meters, except for radial WSW, for which the de-

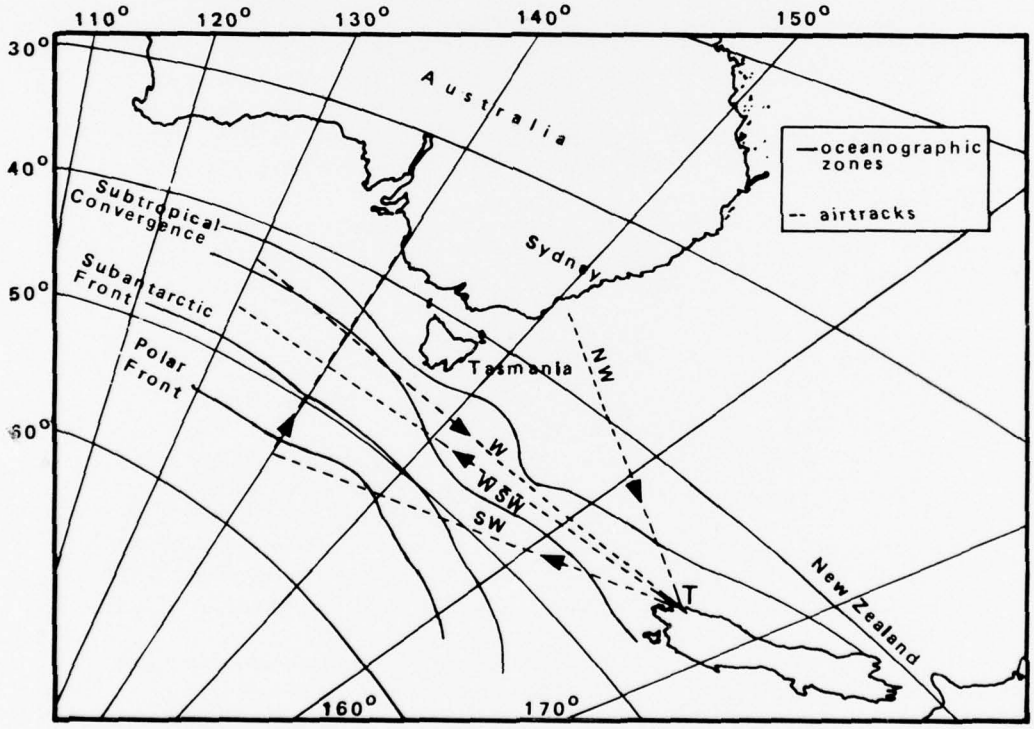

Figure 1. Approximate location of principal oceanographic features in the South Tasman Sea and Southeast Indian Ocean. Dashed lines indicate acoustic propagation paths investigated during Project Tasman Two.

tonation depth was 914 meters. Two additional drops at 18 meters were made along the eastern half of radials NW and W. The aircraft tracks are shown in Fig. 1.

Following the SUS drops, the research ship Tui made an oceanographic cruise along radial W as far as 155°E and then returned to New Zealand along the complete length of radial NW. Bathymetry was recorded continuously and velocity-temperature-depth or salinity-temperature-depth lowerings were made at intervals of approximately 100 km on each radial. In addition, the Australian research ship HMAS Kimbla undertook an oceanographic cruise over the large bathymetric feature south of Tasmania known as the South Tasman Rise. The oceanographic and bathymetric data obtained on these cruises have been compiled, together with relevant historical data, to form a fairly complete picture of the environmental conditions along each radial (Ref. 3).

Figure 1 also illustrates the main oceanographic features of the region. The oceanographic conditions in the area have been summarized by Gordon (Ref. 4), but a brief description is relevant here: The Subtropical Convergence, which forms the boundary between the relatively warm, saline subtropical water to the north and the subantarctic waters of the south, lies in a broad band approximately along 45°S. From an acoustician's point of view this feature marks the development of a relative maximum in the sound-speed profile at a depth of about 500 meters. This maximum is fully developed at the southern boundary of the Subtropical Convergence and persists to the south until it disappears at the Australasian Subantarctic Front near 50°S. South of the latter feature, the sound-speed minimum rises steadily from an initial depth of about 1250 meters to near-surface depths at about 55°S. The disappearance of the deep sound channel marks the location of the Polar Front. The change of axis depth is related to the depth of the salinity minimum produced by cold, relatively fresh antarctic intermediate water, which sinks and flows northwards at the Polar Front.

ENVIRONMENTAL DATA

The oceanographic and bathymetric conditions along the three radials studied here are summarized in Fig. 2, 3, and 4, as functions of distance from point "T". As a general rule, the continental shelf falls away steeply from the New Zealand coast for all three radials, and depths of 4000 to 4500 meters are reached within 30 km.

Radial NW (Fig. 2) exhibits the most uniform bathymetry once clear of the continental slope. The average depth is about 4500 meters and there are no intrusions above 3000 meters. The sound-speed profiles near the New Zealand coast are typical of the Subtropical Convergence in summer, with surface sound speeds near 1510 m/s and an inflection point at about 500 meters. This latter feature is present only in profiles measured out to about 1000 km. At greater ranges the sound-speed profiles are more typical of warmer subtropical waters, as indicated by the rapid increase of surface sound speed, which reaches a maximum of 1530 m/s near Sydney. As is shown later, the rather subtle

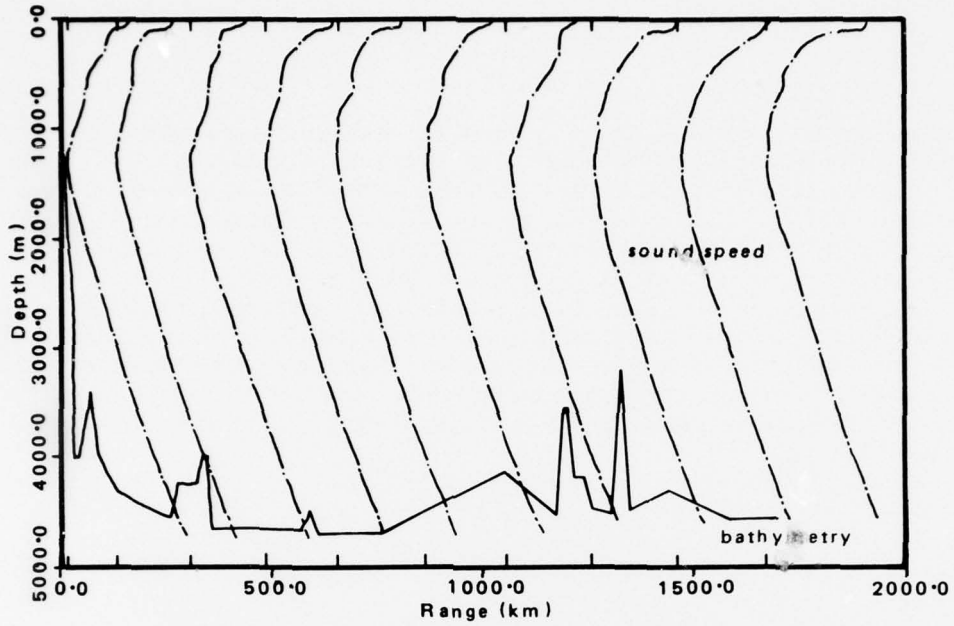

Figure 2. Radial NW showing bathymetry and sound speed profiles. The tic marks indicate the range at which the profile was measured and correspond to a sound speed of 1485 m/sec.

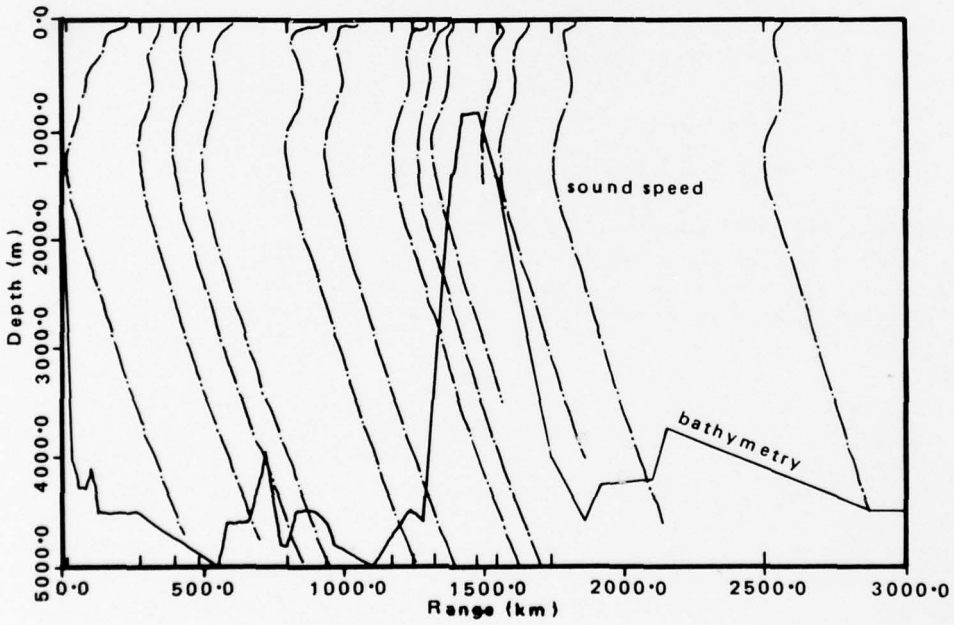

Figure 3. Radial WSW showing bathymetry and sound speed profiles. The tic marks indicate the range at which the profile was measured and correspond to a sound speed of 1485 m/sec.

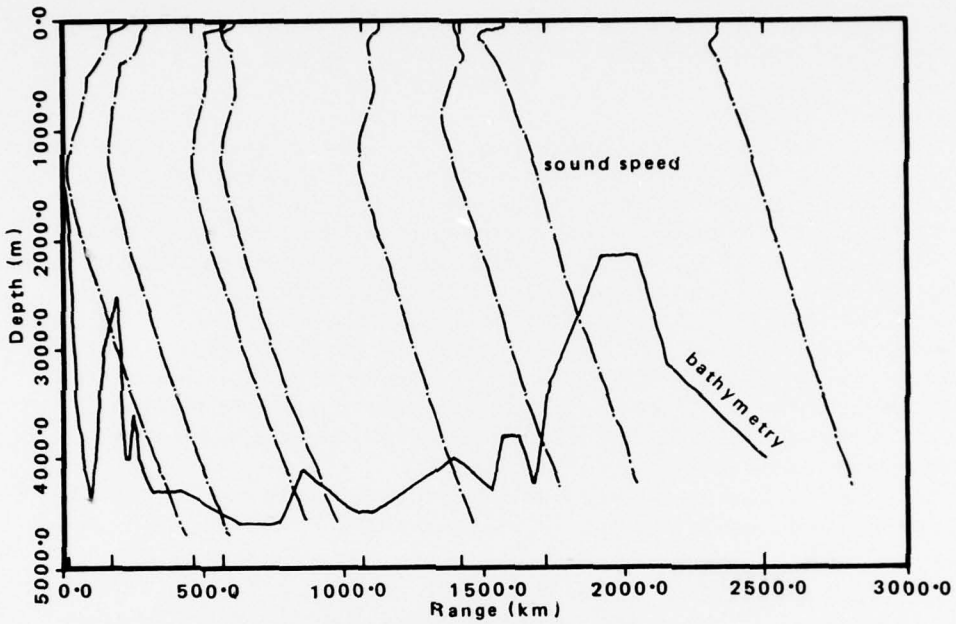

Figure 4. Radial SW showing bathymetry and sound speed profiles. The tic marks indicate the range at which the profile was measured and correspond to a sound speed of 1485 m/sec.

change in sound-speed profile seen here has a marked effect on the predicted acoustics of the region.

The bathymetry of radial WSW (Fig. 3) is dominated by the South Tasman Rise. This large feature is approximately 500 km across at the base and rises to a minimum depth of 850 meters. Except in the vicinity of the New Zealand coast the oceanographic conditions along this radial are typical of Australasian subantarctic waters. The surface sound speed is usually less than 1500 m/s and the profile exhibits a relative maximum near 500 meters.

The SW radial (Fig. 4) has several interesting features. Four different oceanographic regions can be identified on the basis of sound-speed profile. The Subtropical Convergence region is seen to extend out to about 450 km, after which subantarctic conditions prevail until the Australasian Subantarctic Front is reached at a range of approximately 1400 km. The channel axis then rises over the following 200 km until the deep sound channel disappears at about 1600 km. Just south of this point (the Polar Front) the surface sound speed drops by about 20 m/s to 1465 m/s. Apart from the continental slope, the bathymetry is dominated by two major features: the first feature, known as Resolution Ridge, rises to a minimum depth of 2500 meters at a range of about 200 km. The

second, much more extensive feature forms part of the Southeast Indian Ridge (Ref. 5) and rises about 2000 meters at a range of 2000 km.

ACOUSTIC DATA

The received shots were recorded broadband on analog tapes which were returned to the Defence Scientific Establishment for analysis. Each signal was subsequently bandpass filtered through 1/3 octave filters at 16, 31.5, 63, 125, 250, 500, and 1000 Hz. After the signals were processed by an analog squarer-integrator to obtain the energy of each shot, propagation loss versus range curves were produced for each frequency band using source levels interpolated from curves given by Urick (Ref. 6). The best quality data were obtained in the 125 and 250 Hz bands because of the depth of the shots. The two lowest frequency bands were poor because of the relatively weak source level and high ambient noise conditions at this particular site. The unexpectedly high ambient noise level was thought to be associated with the active surf conditions experienced near the hydrophones, which were placed within 2 km of the coastline.

The Tasman Two data set is available in the Naval Sea Systems Command ocean environmental acoustic data bank (NAVDAB) system (Ref. 7).

SEDIMENTARY STRUCTURES

Detailed data on the properties of the sediment cover in this area are sparse. In general, the total sediment depth is found to be of the order 100 meters on the continental shelf and South Tasman Rise and to be of the order 1000 meters in the ocean basins.* Several boreholes drilled during Leg 29 of the Deep Sea Drilling Project (Ref. 8) have been used to obtain quantitative spot estimates of sediment composition. In addition, Houtz compared the Deep Sea Drilling Project data with seismic reflection profiler results and thereby extended the coverage away from the immediate vicinity of the boreholes (Ref. 9 and 10). Following Hamilton (Ref. 11) these data have been used to construct geoacoustic models of the sediment structure for each radial. Details of the models are included in the discussion of results.

PROPAGATION LOSS CALCULATIONS

SUMMARY OF PARABOLIC EQUATION METHOD

The parabolic equation method was first applied to underwater acoustics problems in 1973 by Tappert (Ref. 2), although a comprehensive discussion of the technique has only recently been published (Ref. 12). The essentials of the method are as follows: Sound propagation in the ocean is governed

---

* Personal communication from F. J. Davies, Geophysics Division, 1975.

by the wave equation for the acoustic pressure excess, p:

$$\Delta^2 p + k_0^2 n^2(r,z)\, p = 0 \tag{1}$$

where the wavenumber at some reference sound speed, c_0, and angular frequency ω, is given by

$$k_0 = \omega / c_0 \tag{2}$$

and the refractive index is given by

$$n(r,z) = c_0 / c(r,z) \tag{3}$$

The index is assumed to vary only with depth, z, and range, r. The method is, however, applicable to cases for which the environment varies in azimuth as well.

If n depends on depth only, Eq. 1 may be solved as a boundary value problem using well-known techniques (Ref. 13). The solution is given in terms of a complete set of cylindrical waves, $p_m(r,z)$, known as "normal modes." These waves take the general form

$$p_m(r,z) \approx N_m (k_m r)^{-1/2} U_m(z) \exp(i k_m r) \tag{4a}$$

where N_m is a normalization factor, k_m is the horizontal wave number and $U_m(z)$ gives the pressure amplitude as a function of depth. This function is oscillatory and has m phase reversals. The approximate depth increment between these phase reversals can be obtained from the "vertical wave number," K_m, defined by

$$K_m = (k_0^2 - k_m^2)^{1/2} \tag{4b}$$

The above approach cannot be applied to range-dependent environments. Instead, one of several approximate methods must be used. The simplest approximation is based on the assumption that any horizontal gradients are too weak to induce significant mode coupling; the modes are said to propagate adiabatically (Ref. 14). This means that acoustic energy initially coupled to a given mode remains carried by that mode as it adjusts to the changing environment. This method may be implemented by recalculating the normal modes for each new environment and replacing the phase by its integral over range. This approach is ideally suited to deep ocean situations where the bathymetry is unimportant. However, it has been applied in modified form to shallow-water situations (Ref. 15 and 16).

The basis for the parabolic equation approximation is to assume that the total pressure field, p, has the form

$$p = U(r,z)r^{-1/2} \exp(ik_0 r) \tag{5}$$

where it is assumed that most of the range dependence is represented by the second term and that $U(r,z)$ changes only slowly with range. The "parabolic" approximation to the wave equation can be derived by substituting Eq. 5 into Eq. 1. A useful form of this approximation is

$$-2ik_0 \frac{\partial U}{\partial r} \approx \frac{\partial^2 U}{\partial z^2} + k_0^2 [n^2(r,z) - 1] U \tag{6}$$

which is valid provided the following conditions hold:

$$k_0 r \gg 1 \tag{7}$$

$$\left| \frac{\partial^2 U}{\partial r^2} / 2ik_0 \frac{\partial U}{\partial r} \right| \ll 1 \tag{8}$$

The first condition is the usual for field approximation, which is easily satisfied in the ocean. It can be shown that the second condition (Eq. 8) amounts to a "small-angle" approximation (Appendix). Fitzgerald (Ref. 17) has shown that Eq. 6 is valid for a small cone of angles which may be oriented in any direction. The mean angle is determined by c_0, and, in order to minimize the error, it is usual to select a value midway between the maximum and minimum sound speeds encountered.

These approximations convert the boundry value problem to an initial value problem. In other words, given the function U at some range, r_0, Eq. 6 can be used to "march" the solution out to ranges greater than r_0. This technique can be implemented by making use of the so-called "split-step Fourier algorithm" developed by Tappert and Hardin. A detailed derivation is given in Ref. 12 and we quote only the result here:

$$U(r + \Delta r, z) \approx \exp[ik_0 (n^2 - 1)] \frac{\Delta r}{2} F_s^{-1} \left\{ \exp\left(\frac{is^2 \Delta r}{2k_0}\right) F_s[U(r,z)] \right\} \tag{9}$$

The symbols F_s and F_s^{-1} denote the Fourier transform into "S" space and its inverse, and Δr is the range increment.

The following comments hold regarding the usefulness of Eq. 9 and the parabolic equation method in general:

Accuracy. Equation 9 is an exact solution to Eq. 6 (which itself is an approximation to the wave equation) only if the refractive index is a constant (Ref. 12). However, vertical changes of sound speed are typically less than 5% and strong near-surface horizontal sound-speed gradients are of the order 10^{-1} m/s/km (Ref. 14). On this basis it is assumed that Eq. 9 gives a valid solution to the wave equation for a real ocean.

Density. The parabolic equation method does not take the density change at the water-sediment interface into consideration. Thus, a somewhat greater bottom reflection loss than normal is to be expected. However, numerical results indicate that the difference is small. For example, a density contrast of 1.25:1 causes a decrease in reflection loss of less than 0.5 dB/bounce at low grazing angles. In contrast, a 5% jump in sound speed at the sediment interface causes a 4 to 5 dB decrease for the same case (Fig. 5). Thus, the inability to include density in the model is unlikely to be a source of serious error.

Sampling Rates. The numerical solution of Eq. 9 relies on the use of the fast Fourier transform to advance the solution in range at a rapid rate. However to avoid error care must be taken to sample the pressure field with a vertical step-size, Δz, which is ideally about 1/5 the minimum vertical "wavelength" present. This sets a practical upper limit to the number of modes (and thus the frequency) that can be handled, because the computer run-time increases as $n \log(n)$ where n is the number of fast Fourier transform points. Similarly the horizontal step-size, Δr, is limited by the frequency and magnitude of horizontal gradients. However there appears to be no deterministic criteria which can be

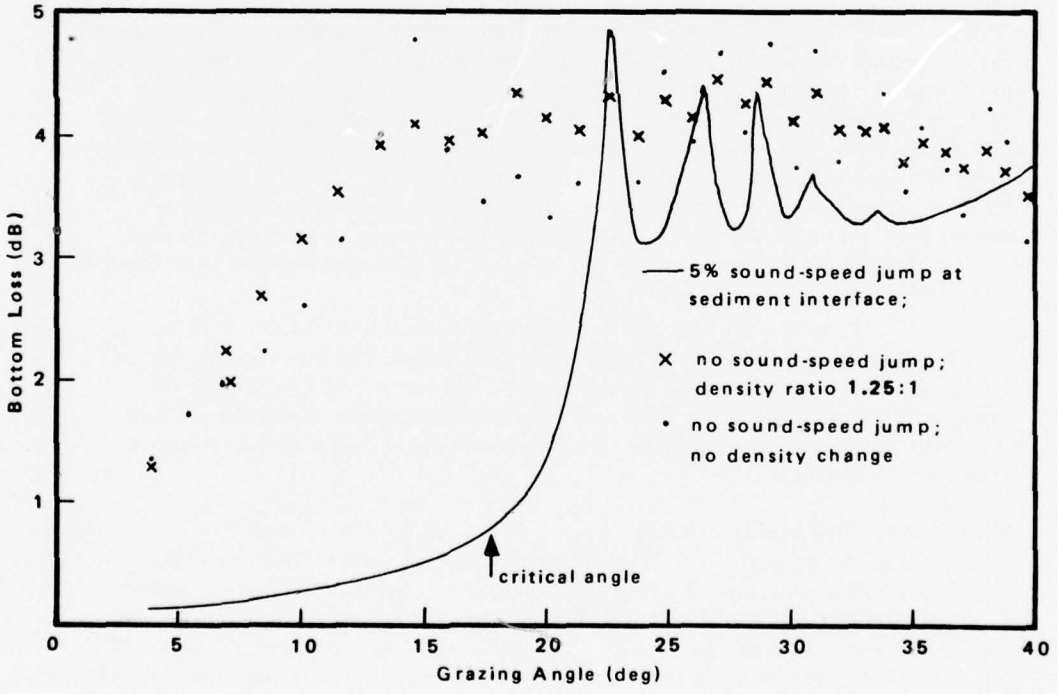

Figure 5. Bottom reflection loss obtained from normal mode program and converted to units of dB/bounce. Water depth 350m. Frequency 63Hz.

applied to establish Δr. Usually a trial and error approach is taken in which Δr is progressively reduced until the solution converges. This implies that in the interests of efficiency parabolic equation computer models need to optimize dynamically both vertical and horizontal step sizes according to the local environmental conditions.

Phase Error. Equation 6 can be used to illustrate the propagation of a single mode under the parabolic equation approximation (Ref. 18). It is found that the mode propagates as:

$$p_m \approx N_m U_m (z) (k_m r)^{-1/2} \exp [i (k_0 - k_m^2 / 2 k_0) r] \qquad (10)$$

Comparing Eq. 10 with Eq. 4a and 4b, it is apparent that whereas the mode amplitude is unaffected, the parabolic equation phase is a first-order approximation of the true phase, $(k_0^2 - K_m^2)^{1/2} r$. Thus in the parabolic equation approximation phase sensitive effects, such as Lloyd Mirror interference patterns, develop a range-dependent offset relative to a normal mode prediction.

Reciprocity. It is well known (Ref. 13) that the normal mode solution, which is valid for environments with no horizontal gradients, is invariant under the exchange of source and receiver coordinates. This phenomenon is known as "reciprocity." When the medium is range dependent it is still theoretically true that reciprocity holds. Experience with ocean fronts indicates that reciprocity does hold to a good approximation in deep water, even in regions of extreme horizontal gradient.* Therefore, reciprocity is assumed to hold for the radials in in Tasman Two. Accordingly all predictions are for a bottomed source radiating from the hydrophone site to a towed receiver at the shot depth. This greatly reduces the computer runtime because the only alternative is to calculate the propagation loss back to the hydrophone from each point of interest. In fact, some differences between up-slope and down-slope calculations have been observed and are discussed in the next section.

Cost. The time required to make parabolic equation runs is known to be high and can be a limiting factor in its use. The longer runs reported in this report required roughly 1/2 to 1 hour each on the Univac 1110 at a cost on low priority time of $200 to $400. The longest times were required for those runs over the South Tasman Rise, which required small horizontal step size, as is discussed elsewhere.

PROGRAM CONSIDERATIONS

The parabolic equation model used was a modified version of an existing NOSC computer program. The modified program accepts an unlimited number of input sound-speed profiles at specified ranges and linearly interpolates the refractive index between the two profiles which straddle the current range. Similarly, the bathymetry is represented as a sequence of linear segments between the input depth-range data points.

* Personal communication from M. A. Pedersen and D. F. Gordon, 1975.

The magnitude of both the range increment, Δr, and the jump discontinuity in sound speed at the sediment interface can also be specified as a function of range. However the specification of the bottom model (sediment type and thickness) is a constant for each run. If necessary, the bottom model can be changed by first generating a new initial pressure distribution at a given range and then rerunning the program to greater ranges with the new sediment structure. Similarly, the depth increment Δz cannot be changed without re-starting the program.

Initial pressure distribution functions, $U(r_0,z)$ (which are referred to as "starters"), were calculated using both normal modes and rays. In deep water it is usual to start the parabolic equation model with a Gaussian-shaped initial pressure distribution close to the source. The Gaussian shape is used because it filters out high-angle energy (which would be lost at short range anyway) and prevents aliasing of this energy into low angles during the fast Fourier transform sampling process. However, this technique was not suitable to start the Tasman Two predictions because, under the assumed conditions of reciprocity, the "source" was placed on the bottom in shallow water at the top of the continental shelf.

The mode-generated starters involve two approximations (Fig 6a): (1) it is

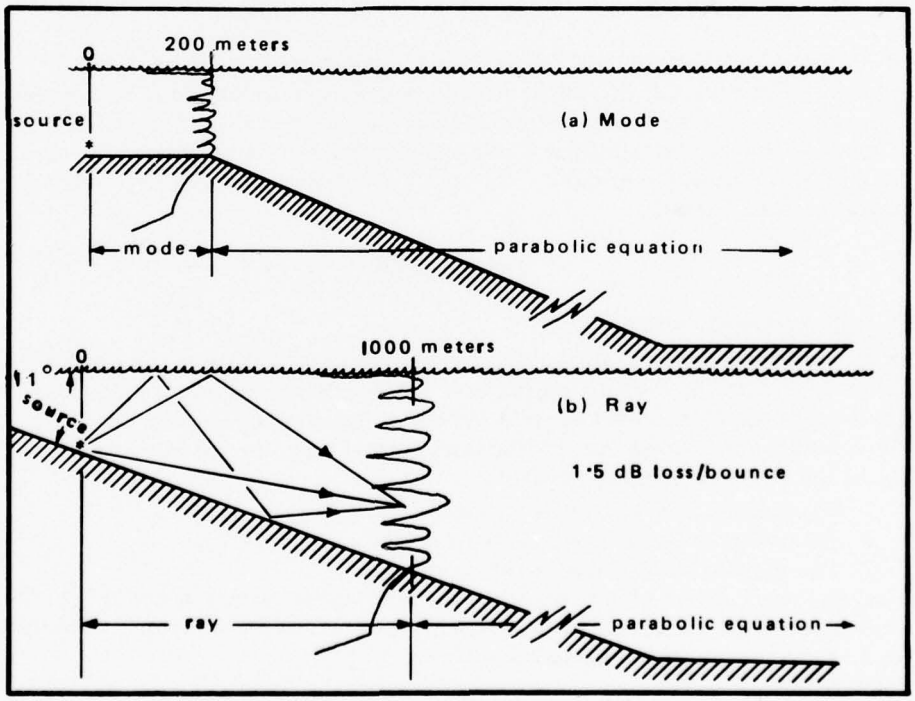

Figure 6. Techniques used to start the parabolic equation.

necessary to assume the water depth is constant at the top of the continental slope in order to apply mode theory; and (2) numerical difficulties impose an upper limit of about 60 degrees to the equivalent ray angle.* The latter approximation restricts the minimum range at which the mode starter is accurate to about 200 meters. Thus, the bathymetry was held at a constant depth of 350 meters for a distance 200 meters down range from the source.

The ray starter was used in an attempt to reduce these approximations.** A constant bottom slope appropriate to the radial concerned was applied near the source (Fig 6b), and the pressure distribution at 1 km was calculated assuming a constant 1.5 dB/bounce reflection loss. This figure was based on the results of mode calculations for various bottom models. Rays in the forward direction up to ± 90 degrees where included.

It is of course, necessary to consider very high angle energy close to the source, because the angle is considerably reduced during propagation down the slope. Ignoring the intermode coupling caused by the bathymetric gradient, the minimum requirement is that energy which insonifies convergance zones when it reaches deep water must be treated properly at the top of the slope. On this basis, the vertical sample interval may be expressed as

$$\Delta z \approx 2H/5m \tag{11}$$

where H is the water depth and m denotes the highest order mode required in deep water. For example, at 100 Hz it is necessary to consider about 150 modes in deep water to include some bottom bounce energy. For a water depth of 4500 meters, Eq. 11 indicates that a step size of 12 meters is adequate. However at the top of the continental slope where H is only 350 meters, the step size is reduced to about 1 meter.

DISCUSSION

PROCEDURES AND FINDINGS

In view of the anticipated difficulties associated with initializing the parabolic equation model on the continental slope, it was decided to attempt predictions of the average signal level over the radials before investigating specific details of the acoustic data. Consequently the initial effort was directed towards a study of the effect on absolute level of:

1. The vertical and horizontal step sizes
2. The sedimentary structure of the bottom
3. The specification of starter functions

Subsequent work reported here discusses the convergence zones of radial NW, the acoustic shadow of the South Tasman Rise, and some distinctive acoustic features related to changes in the sound-speed profile.

* Personal communication from D.F. Gordon, 1975.

** Personal communication from R. White and D.F. Gordon, 1975.

GEOACOUSTIC MODELS

Various geoacoustic models were investigated before selecting the one we refer to as a sediment bottom (Fig. 7). The constraints which led to this model being adopted were:

1. In the absence of firm data on the sedimentary structure of the continental shelf, the model should not be too detailed.
2. The model should utilize accepted parameters to specify the acoustic properties of sediments, such as those given by Hamilton (Ref. 11).
3. In view of the inability to change the bottom model with range, the model should be capable of describing the deep ocean basins.
4. The model should be compatible with the requirements of the normal mode program used to generate starters.

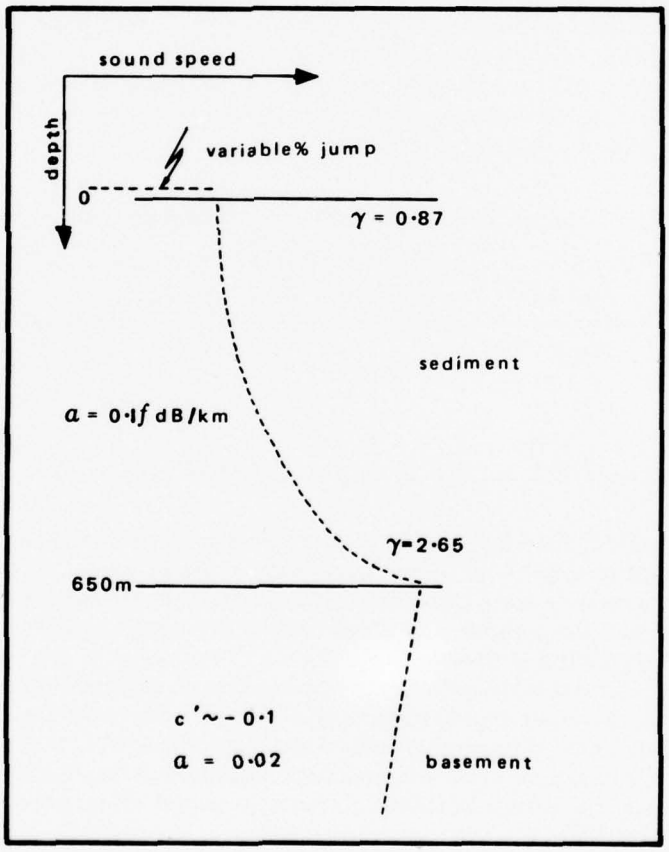

Figure 7. Important parameters of sediment bottom model.

The bottom was therefore represented as a series of fluid layers, in each of which the sound speed varies as

$$c(z) = c_i [1 - 2\gamma_i (z - z_i) / c_i]^{-1/2} \qquad (12)$$

where C_i and γ_i are the sound speed and sound-speed gradient at the top of the ith layer and z_i is the layer depth. Equation 12 is useful in that the normal modes can be expressed in terms of Airy functions, but is limited in that the derived sound speed and gradient take on physical values over a restricted depth range only. Accordingly c_1 was set to the measured value at point "T" and the remaining parameters specified as in Table 1. The layered structure has no direct experimental significance, being imposed to ensure a smooth progression of sound speed and gradient with depth, within the limitations of Eq. 12, and in addition, to ensure that solutions for many high-order modes could be found. The negative gradient in the 5th layer is necessary to satisfy the mechanics of the mode program and has no effect on the solution, as it is at a depth well below that to which acoustic energy penetrates at a significant intensity.

Table 1. Bottom layer parameters for the sediment model.

i	C_i (m/s)	γ_i (s)$^{-1}$	z_i (m)	a_i (dB/km)
1	1499.1	0.87	0	$0.1f_{Hz}$
2	1650.0	1.0	150	$0.1f_{Hz}$
3	1825.0	1.6	300	$0.1f_{Hz}$
4	2125.0	2.6	450	$0.1f_{Hz}$
5	3000.0	-0.1	650	$0.1f_{Hz}$

To compensate for the inability to include density in the model and to allow for greater bottom reflectivity on the continental slope as compared with the ocean basins, a variable jump discontinuity was applied at the water-sediment interface. Usually this jump was taken as 11% on the slope but was tapered to zero on reaching the ocean basins.

Finally, the attenuation coefficient in the bottom, a, was taken as a constant $0.1f_{Hz}$ dB/km, corresponding to a porosity of 65% or greater (sand-silt-clay or finer grain sediment). However because of the jump discontinuity allowed at the surface, it is recognized that this approach is somewhat unphysical in view of the well-known empirical relationships between sound speed, porosity, and attenuation (Ref. 11).

ABSOLUTE LEVELS

To begin the study of absolute signal levels, we investigated the use of the parabolic equation model in an environment similar to that near the hydrophone site. This was modeled as a sound channel having a constant depth of 350 meters overlying a sediment bottom. The sound-speed profile was as measured at point "T". Figure 8 presents a comparison of the normal mode prediction and the parabolic equation prediction. The latter was initialized by the mode solution at 200 meters and marched out with a range increment of 10 meters and a depth increment of 12 meters. Apart from the phase difference of about 500 meters, the predictions are very close at ranges greater than about 2 km. Investigation of the mode solution showed that fewer than 10 modes contributed at these ranges, in which case the 12-meter sample interval is expected to give an accurate solution. At short ranges where many modes contribute, the agreement is not as good.

Turning to the experimental situation, we consider radial NW, which has the simplest environmental conditions at short range. Figure 9 summarizes the best results obtained using the sediment bottom model at 63 Hz. Three

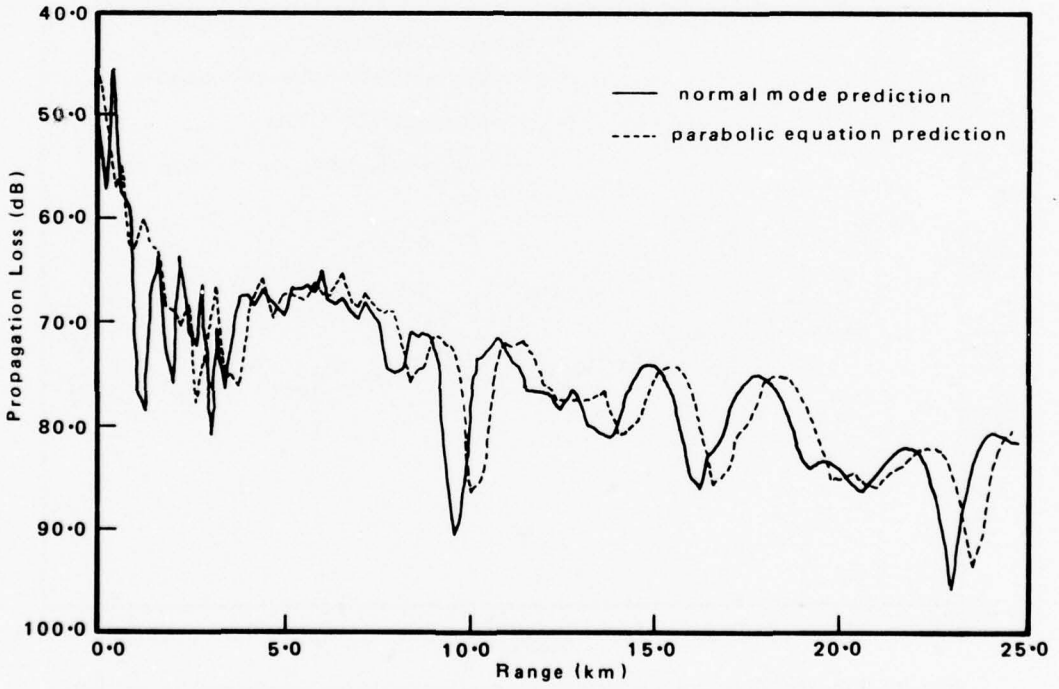

Figure 8. Comparison of predicted propagation loss in shallow water channel overlying sediment bottom. Water depth 350 meters, frequency 63 Hz. No density change at sediment interface.

cases are illustrated: curve **a** was derived using a normal mode starter at 200 meters with Δz initially 6 meters but doubled to 12 meters at a range of 20 km (water depth 2000 meters). Δr was 10 meters down the shelf and 200 meters in deep water. An 11% jump in sound speed at the sediment interface was applied on the shelf out to a range of 27 km. This was tapered to zero over the following 3 km. Propagation loss was calculated at 2-km intervals but is presented as a 5-point average in order to smooth the curve.

Comparison of this curve with the experimental data shows that the predicted level is about 5 dB lower than the measured level. Although this could be due to a source-level error, we observe that the prediction obtained using a 12-meter vertical sample throughout (curve **b**) is significantly different in detail. This is an indication that the solution has not stabilized, most probably because Δz needs to be reduced further. Assuming about 60 significant modes in deep water at 63 Hz, Eq. 11 indicates that Δz should be less than 3 meters at the top of the shelf. Unfortunately it was not possible to run the existing model for Δz this small without further modification to the program.

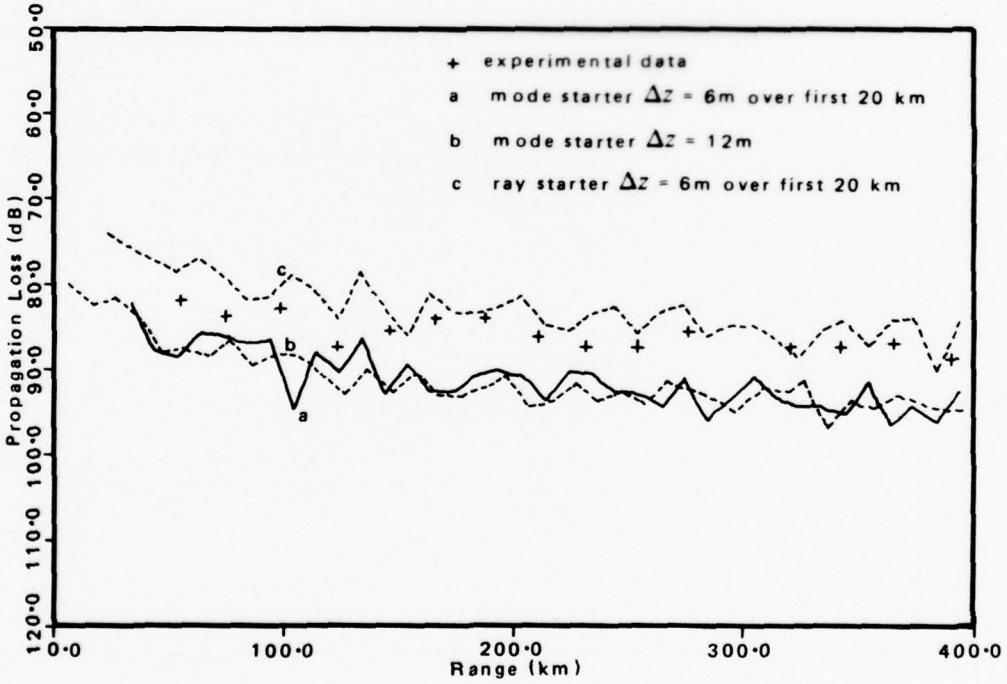

Figure 9. Radial NW. Comparison of parabolic equation propagation loss predictions with experimental data at 63 Hz.

However checks were made on some of the other parameters of interest: To investigate the effect of different sediment structure, the prediction was run down the slope with a bottom modelled by a sediment layer 100-meters thick, porosity 65%, attenuation coefficient $0.1f_{Hz}$ and sound speed jump 3.3%, overlying basement rock. The predicted level (not shown) was about 5 dB lower than curve **a**, presumably because of increased absorption within the sediment due to the reduced bottom reflectivity. It is interesting that the presence of the strongly reflecting layers of basement rock (sound speed 5000 m/s) did not raise the signal level. This indicates that little acoustic energy penetrates as far as the basement, which is at a depth of 4 wavelengths at this frequency, and to some extent justifies the use of the sediment model on the continental shelf.

In addition, a prediction was made with the ray starter which, as discussed earlier, uses a constant-slope approximation to the bathymetry near "I" and includes all initially forward-going energy (curve **c**). The sampling intervals and all other parameters are the same as for curve **a**. We observe that because of the greater water depth at 1 km (600 meters), where the parabolic equation starter

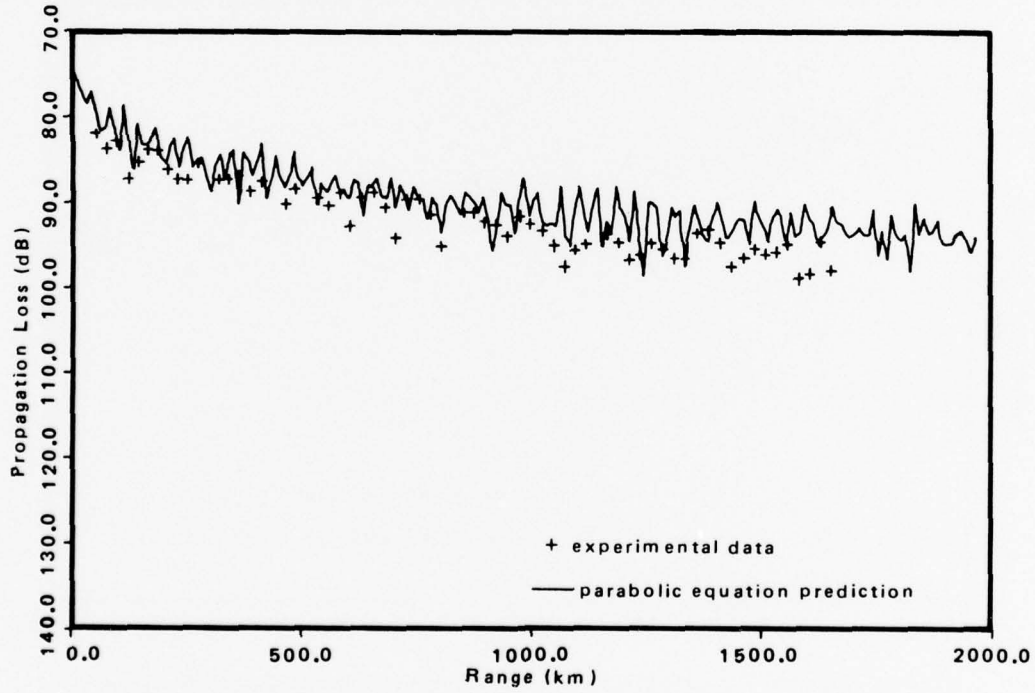

Figure 10. Radial NW: Comparison of parabolic equation propagation loss prediction with experimental data at 63Hz.

is generated, the 6-meter vertical sample interval is a better approximation in this case. Comparing curve **c** with curve **a**, the ray starter yields a predicted level about 9 dB greater than the mode starter. However, the overall level exceeds that of the experimental data by a few dB. A possible cause of this excess level is the simple 1.5 dB/bounce, constant reflection loss model assumed for the ray calculation. From Fig. 5 this low loss would tend to exaggerate the high-angle energy content.

Figures 10 and 11 illustrate the predictions for deep shots, over the complete span of radial NW, at 63 Hz and 125 Hz, respectively. The parabolic equation model was initialized with the ray starter in both cases and apart from frequency, all parameters are as for curve **c** in Fig. 9. These figures represent the best fit to the overall signal levels on this radial. However, in view of the previous discussion it is expected that the degree of agreement would be significantly improved by the use of smaller Δz over the first few kilometers of range and a better reflection loss model when calculating the starter.

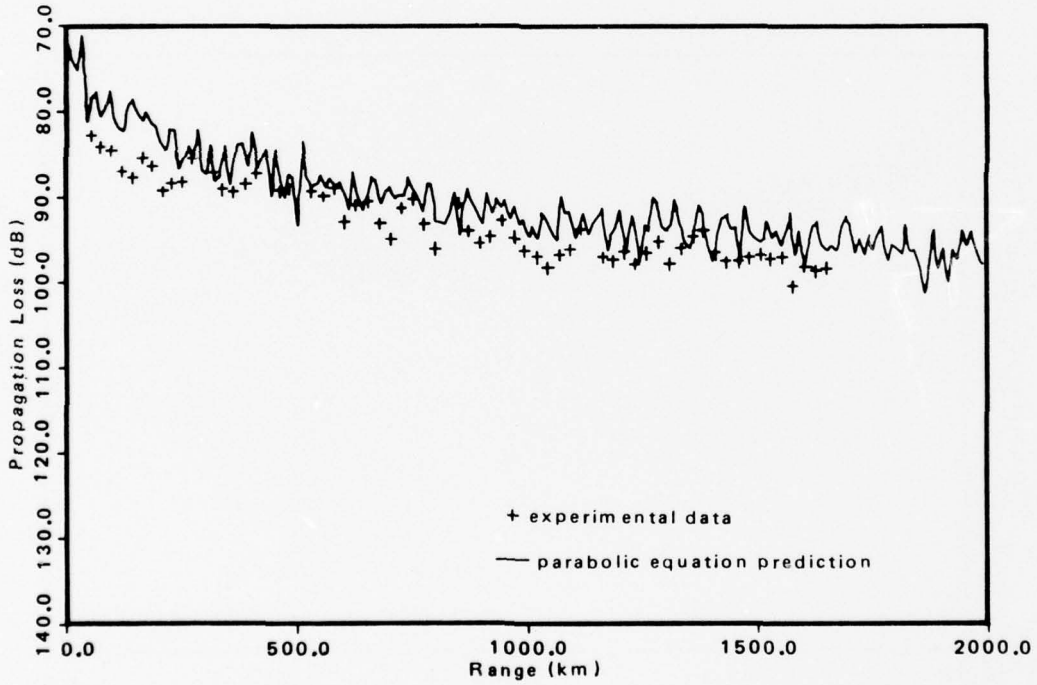

Figure 11. Radial NW: Comparison of parabolic equation propagation loss prediction with experimental data at 125 Hz.

CONVERGENCE ZONES

The acoustic data for the shallow shots on radial NW are interesting in that the convergence zone structure is more pronounced, both in the higher frequency bands and at longer ranges (Ref. 1). Figures 12 and 13 illustrate the convergence zone predictions (18-meter shots) for this radial at 63 and 125 Hz, respectively. These predictions were generated at the same time as those in Fig. 10 and 11. The bathymetry has been superimposed on these figures to indicate the scale of the continental slope, which drops down to the deep ocean within the first convergence zone.

Comparing the experimental and predicted data at 63 Hz, we see that the experimental zones are best defined at ranges greater than 300 km but are about half a zone ahead of the prediction in phase. At 125 Hz (Fig. 13), the measured zones over the first 300 km are better defined than at 63 Hz and compare quite well with the prediction. However as in Fig. 11, the predicted level is too high on the average. At longer ranges the phase difference seen in Fig. 12 is evident here also.

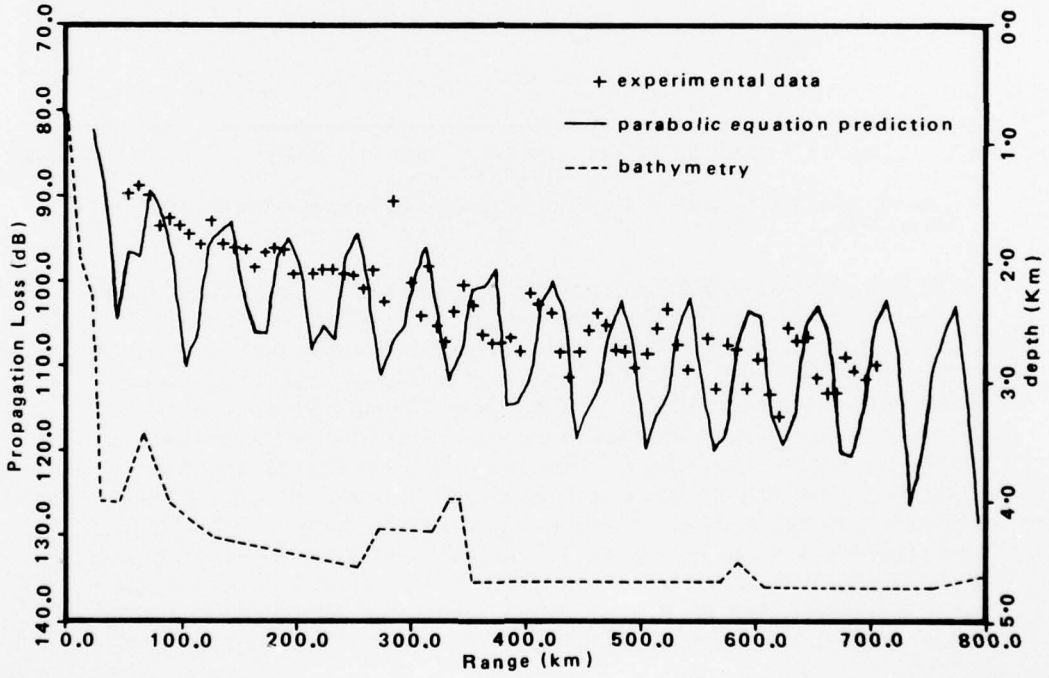

Figure 12. Radial NW: Comparison of predicted convergence zone propagation loss with experimental data at 63 Hz.

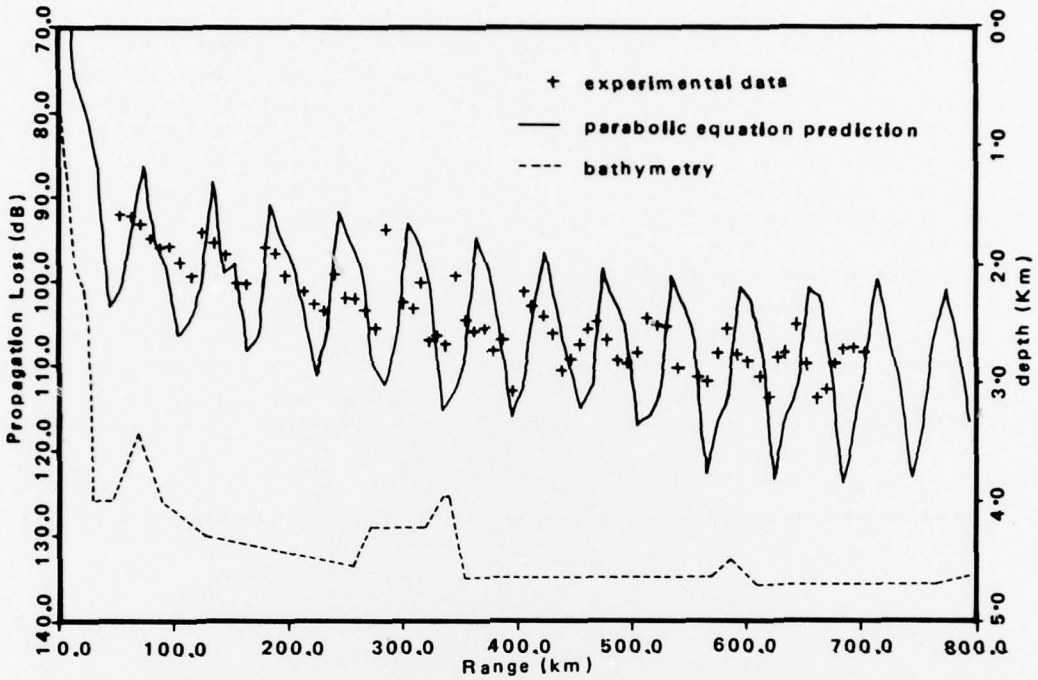

Figure 13. Radial NW: Comparison of predicted convergence zone propagation loss with experimental data at 125 Hz.

The most significant difference between the data and the predictions is that the predicted level drop between peak and shadow is about twice that measured. Acoustic energy is of course carried into the shadow zone by bottom-reflected modes. Therefore, the lack of agreement may point to a need for a bottom model with lower reflection loss. It is also possible that sufficient bottom-reflecting modes were not included in the calculation because the vertical sample-size, Δz, was too coarse. A third possible reason for the discrepancy is that we are comparing a continuous wave prediction with data derived from a 1/3-octave energy analysis. However, any smoothing induced by the finite-band analysis is minimal in this case, because the gross features of convergence zones are essentially frequency independent. In view of the operational significance of these effects in areas where refracted-surface reflected (RSR) propagation is marginal, it was unfortunate that the investigation could not be pursued further.

ACOUSTIC SHADOWING

On radial WSW the SUS were set to detonate at a depth of 914 meters, which is just above the axis of minimum velocity but slightly below the peak of the

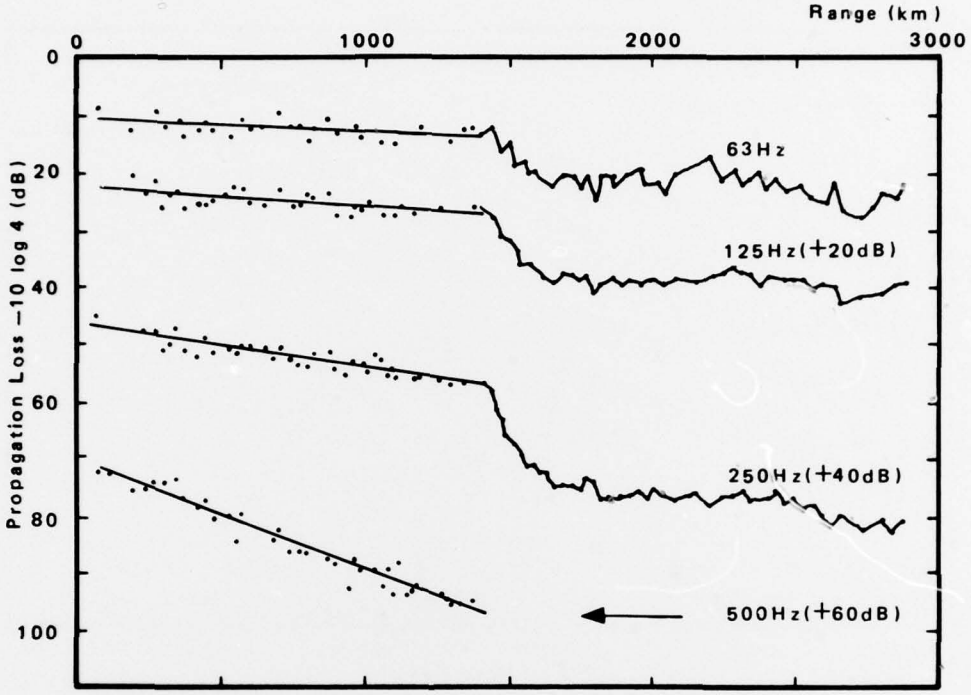

Figure 14. Radial WSW: Experimental data showing acoustic shadow of South Tasman Rise. Reproduced with permission from Ref. 1.

South Tasman Rise. This shoals to a minimum depth of 850 meters (Fig. 3). The principal feature of the acoustic data for this radial is the "shadow" cast by the Rise, which of course does not act as a complete stop, because some acoustic energy is channeled over the top via bottom-reflected paths. By extrapolating the propagation loss data east of the Rise back into the shadow region, the depth of the acoustic shadow can be measured. The shadow at 63 Hz is close to 7 dB (above cylindrical spreading loss) and it increases at a rate of about 4.5 dB/octave over the higher frequency bands (Fig. 14). The data in the 16- and 31.5-Hz bands are of insufficient quality to obtain accurate estimates.

In order to reduce the computer run-time for this radial, two approximations were made. First, the parabolic equation program was initiated at 900 km using a normal mode starter. Consequently the absolute levels predicted in this section are somewhat arbitrary. Second, a fixed sound-speed profile (measured at 1470 km in Fig. 3) was used on the assumption that the bathymetry would dominate the shadowing process. Therefore the only environmental variables here are the bathymetry and bottom model. For each run the horizontal step-size, Δr, was

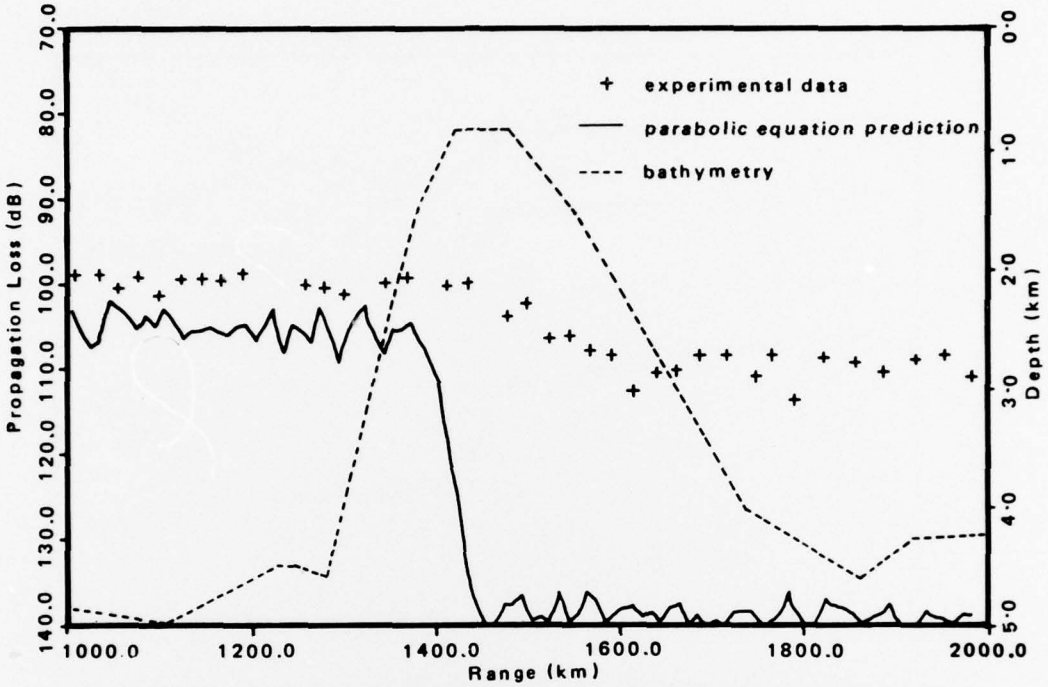

Figure 15. Radial WSW: Comparison of parabolic equation propagation loss prediction with data at 63 Hz. Sediment bottom model with no sound-speed jump at sediment interface.

progressively reduced from 200 meters in deep water (at 63 Hz), to 20 meters at the top of the Rise. At 125 Hz Δr was half these values. However, the vertical sample-size, Δz, was fixed at 12 meters for all cases.

To illustrate the importance of the bottom model in this situation Fig. 15 gives the prediction obtained at 63 Hz using the sediment bottom (Fig. 7) with no sound speed jump at the water-sediment interface. It is apparent that the feature acts as an almost complete acoustic stop, most of the energy being absorbed within the sediments. The bottom loss was reduced considerably by imposing a jump in sound speed at the sediment interface. The magnitude of the jump was tapered from zero either side of the Rise to 11% at depths less than 1500 meters. At 63 Hz this bottom model gives a good fit to the data (solid line in Fig. 16), but it is interesting that at 125 Hz (Fig. 17) the shadow obtained using the same model is not sufficiently deep. The predicted drop in level west of the South Tasman Rise at 125 Hz is, in fact, 5 dB less than that at 63 Hz. The gap in predicted level was caused by the source (or receiver) depth intersecting the sediment at the top of the sea mount.

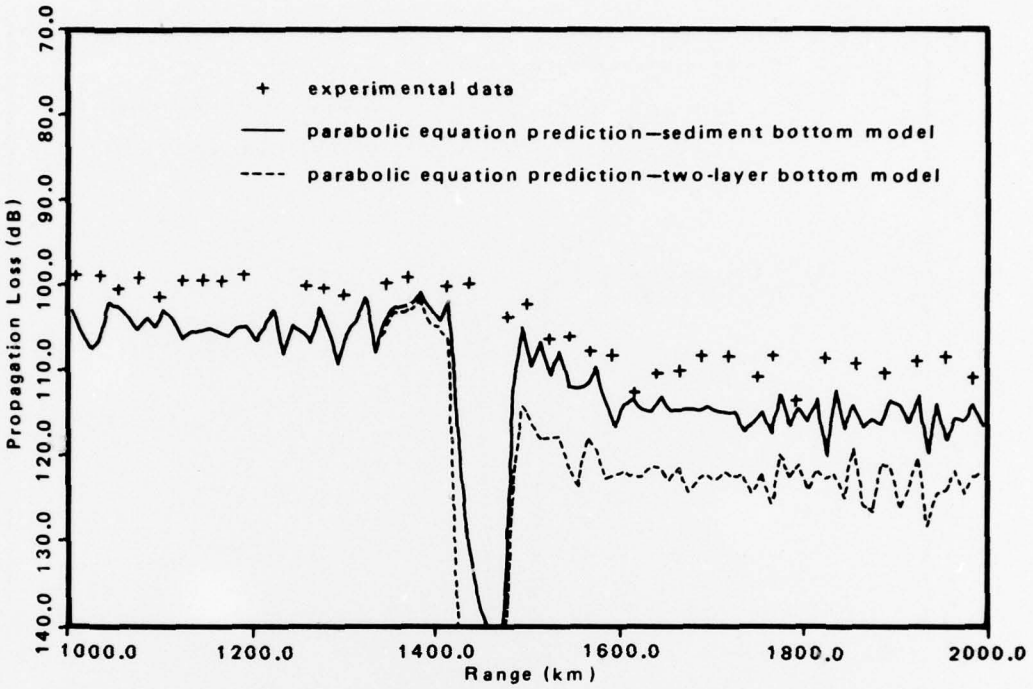

Figure 16. Radial WSW: Comparison using sediment models with sound-speed jumps; frequency 63 Hz.

In an attempt to improve the prediction, we used a more detailed bottom model of the Rise based on seismic surveys of the area and data logged from borehole 281, DSDP Leg 29, which was drilled on the south flank of the South Tasman Rise (Ref. 8, 9, and 10). The model (Fig. 18) consists of a 25-meter layer of strongly absorptive, very fine sand overlying 175 meters of less absorptive, sand-silt-clay. (For this reason it is referred to as the "two-layer" model.) Basement occurs at 200 meters in the model and imposes a 300% jump in sound speed (Table 2).

Table 2. Bottom layer parameters for the two-layer model.

i	c_i (m/s)	γ_i (s)$^{-1}$	z_i (m)	a_i (dB / km)
1	1489.0	1.0	0	$0.5f_{Hz}$
2	1514.7	1.05	25	$0.1f_{Hz}$
3	5500	0.0	200	$0.02f_{Hz}$
4	5500	0.1	700	

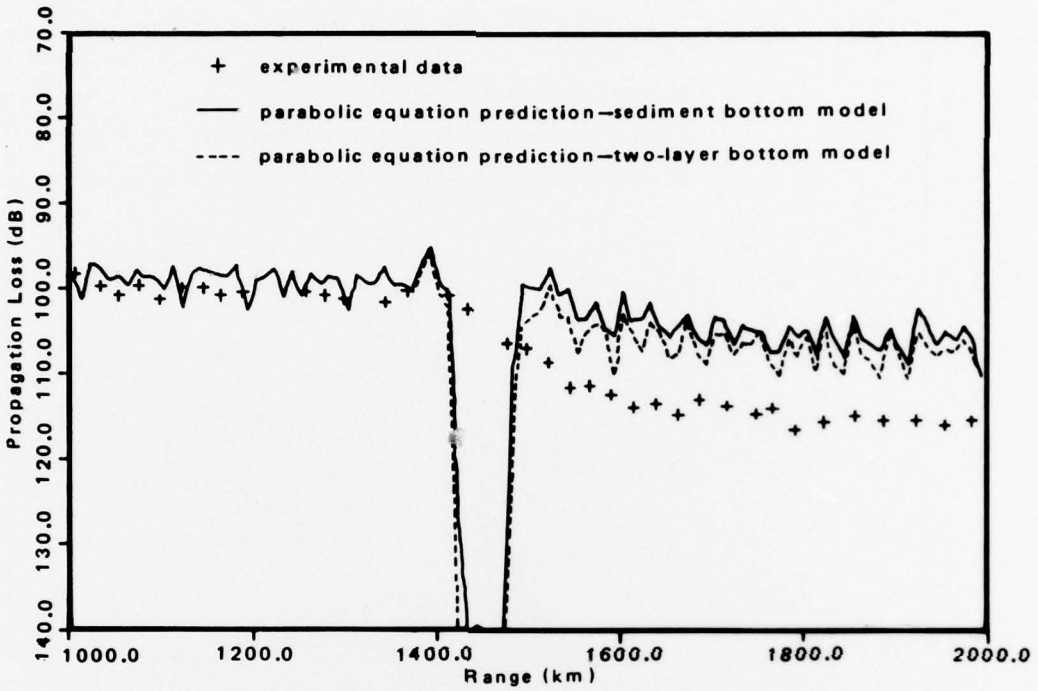

Figure 17. Radial WSW: Comparison using sediment models with sound-speed jumps; frequency 125 Hz.

To implement the necessary changes to the bottom model, the program was run in three stages. First the prediction was run, using the sediment model, from 900 to 1280km, at which point a new starter was stored. The prediction was then run over the South Tasman Rise, using the two layer model, out to 1860 km, where a second starter function was stored. Finally the prediction was continued using the sediment model again.

The results are illustrated by the broken lines in Fig. 16 and 17. We see that the predicted shadow at 125 Hz has deepened and more closely fits the data. However, the shadow at 63 Hz is now considerably deeper than the observed shadow.

These results are encouraging in that both the onset of the shadow and the initial rate of decrease in signal level behind the Rise agree well with the data. At the same time, the results are disappointing in that the predicted frequency dependence of the acoustic shadow is opposite to that observed: For both bottom models the level drop behind the Rise *decreases* with increasing frequency. This discrepancy could be related to the choice of vertical sample size, Δz, which remained constant at 12 meters throughout. At the top of the Rise, where the water depth is 850 meters, a sample size of about 3 meters would be more appropriate at 125 Hz, assuming 120 modes are important (Eq. 11).

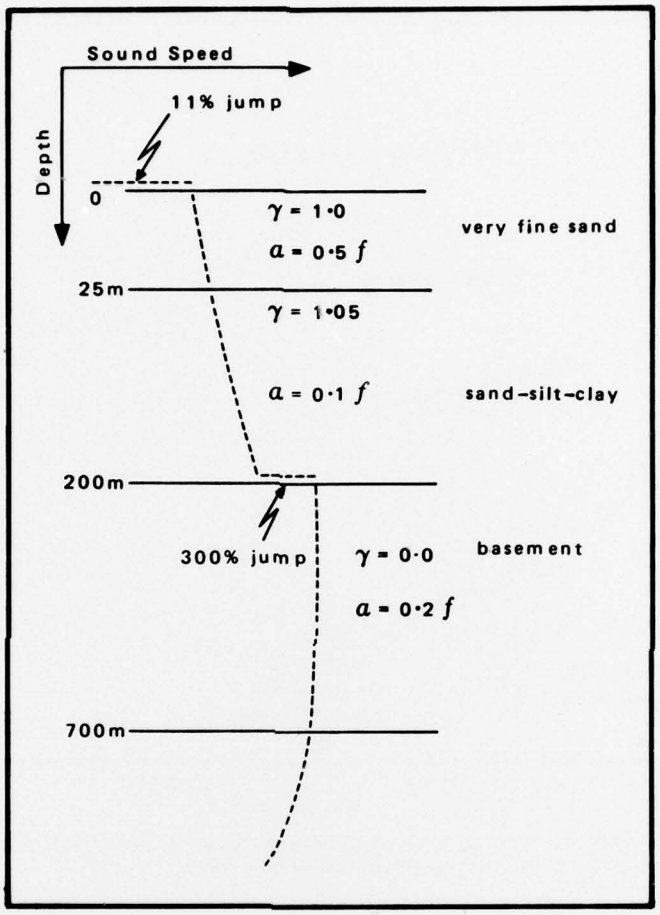

Figure 18. Important parameters of "two-layer" bottom model.

OCEANOGRAPHIC EFFECTS

The acoustic propagation data from radial SW is dominated by the presence of a high-loss region at short ranges. After the effects of cylindrical spreading are removed, the signal levels at ranges greater than 450 km are about 14 dB lower than the levels extrapolated from about 150 km (Fig. 19). In contrast to the frequency-dependent level drop seen west of the South Tasman Rise, the level drop on radial SW appears to be *independent* of frequency. South of this anomaly, two distinct attenuation regimes can be defined. The first regime extends from the acoustic anomaly out to a range of about 1200 km and apparently coincides with the sub-antarctic water mass lying between the Subtropical Convergence and the

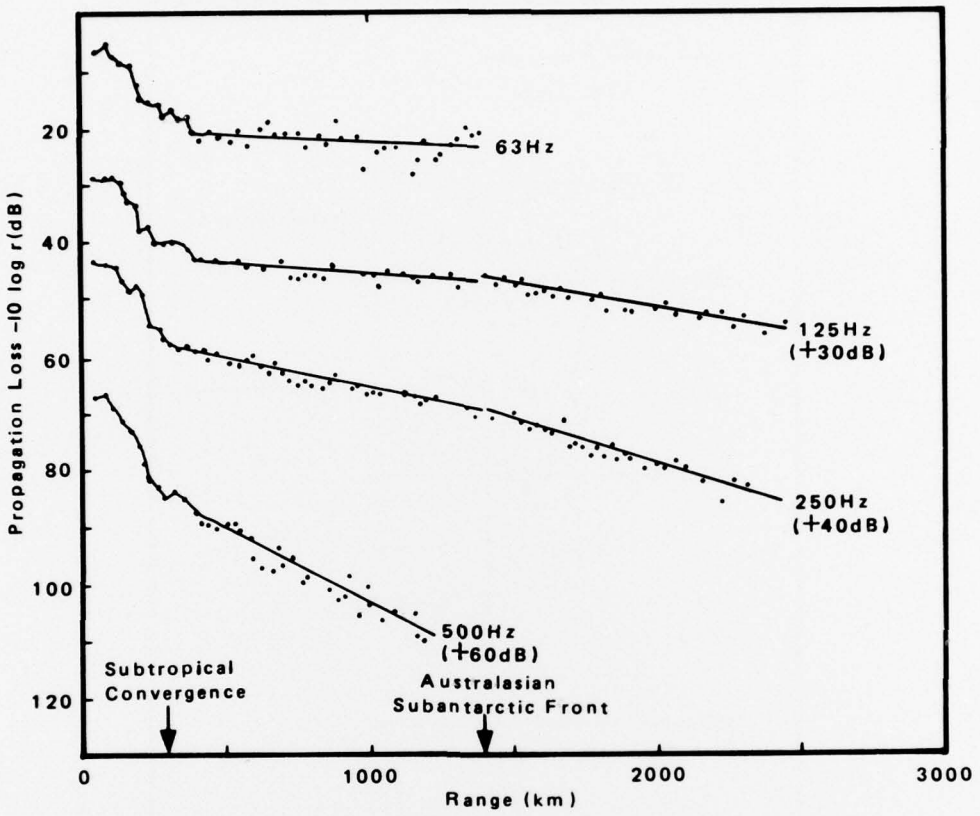

Figure 19. Radial SW: Experimental data showing acoustic anomaly for ranges < 450 km and high attenuation zone south of Polar Front. Reproduced with permission from Ref. L

Australasian Subantarctic Front. The second regime extends southwest from the Australasian Subantarctic Front over the remainder of the radial.

Figure 20 illustrates the parabolic equation prediction at 125 Hz for this radial using the ray starter. The sediment bottom model was used over the entire radial, with an 11% jump in sound speed at the sediment interface on the continental slope. The vertical sample-size was initially 6 meters, but was increased to 12 meters for ranges greater than 20 km. In-shore of the Resolution Ridge at ranges less than 200 km the prediction follows the trend of the data but, as discussed for radial NW, the average level is a few decibels too high. However, just south of the Ridge, where the experimental level is anomalously low, the prediction shows no evidence of a corresponding level drop. The reasons for this are not clear. One possibility is that the Resolution Ridge rises to much shallower depths

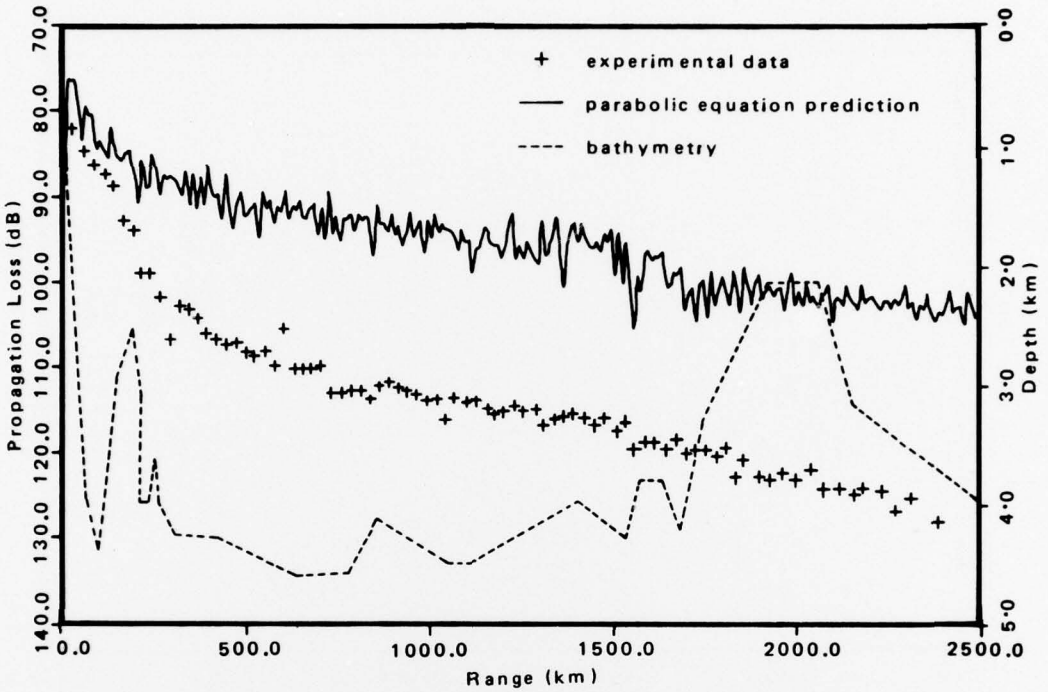

Figure 20. Radial SW: Comparison of propagation loss predictions with experimental data at 125 Hz.

than indicated by bathymetric charts of the area. However, the lack of a frequency dependence similar to the shadow of the South Tasman Rise, raises the interesting possibility that this anomaly is related to some oceanographic property of the area rather than to the bathymetry. The fact that there is no noticeable level drop associated with the Southeast Indian Ridge, a massive feature some 350 meters higher than the Resolution Ridge, lends support to this hypothesis. In any case, it is clear that the environment near the Resolution Ridge has not been adequately represented.

A second interesting feature of this prediction is the change in character that occurs near 1500 km. Evidently this is caused by the disappearance of the deep sound channel at the Polar Front (Fig. 4). However, south of the Polar Front the prediction does not show a marked increase in slope as does the experimental data. It is possible that this increase in attenuation is caused by rough surface effects not included in the model: Presumably any surface-induced coupling of energy into bottom bounce modes would be accentuated in the region south of the Polar Front, because all modes are of the RSR class.

Figure 21 gives the corresponding prediction for an 18-meter SUS on this radial. It is interesting that the average signal level *increases* with range, the

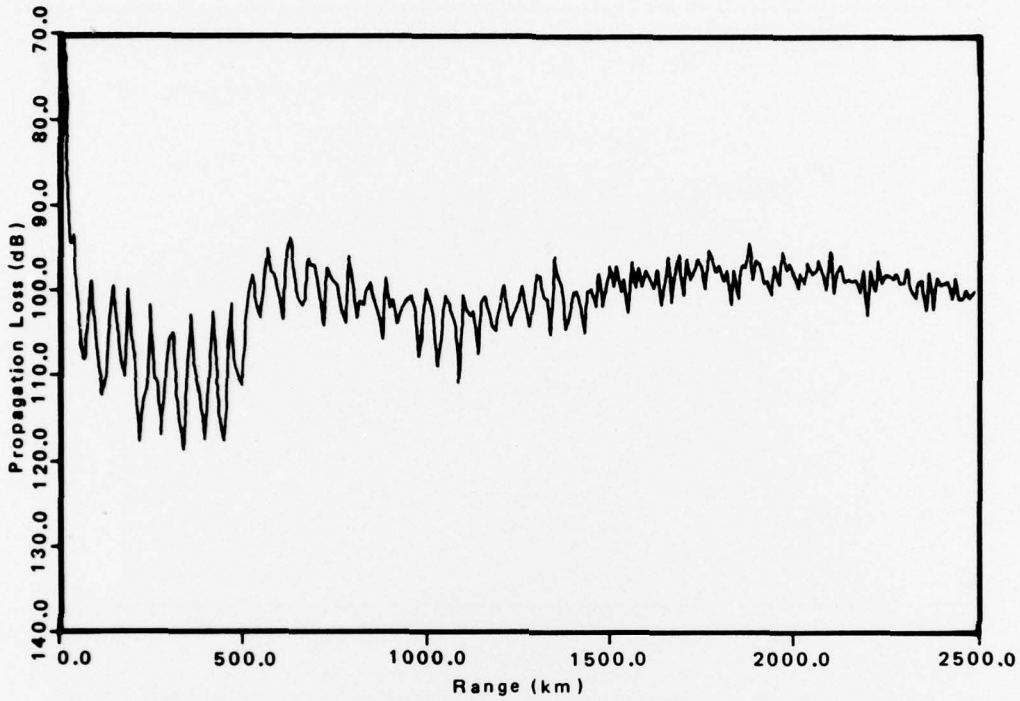

Figure 21. Radial SW: Parabolic equation propagation loss prediction for 18-meter SUS, 125 Hz frequency.

level at 2000 km being some 10 to 15 dB greater than that at 500 km. In addition, we see that the convergence zone structure abruptly disappears at the Polar Front.

As a final example of changes in the propagation characteristics induced by different oceanographic conditions, the predictions at 63 Hz for an 18-meter and a 244-meter SUS on radial NW are shown in Fig. 22 and 23, respectively. These predictions were initialized by the ray starter and run under the same conditions as discussed for Fig. 10. It is interesting that the rather subtle change in profile shape at about 1000 km (Fig. 2), caused by a near-surface trend to warmer temperatures, could have such a dramatic effect on the acoustics: For the 18-meter SUS we find a sudden increase in the slope of the convergence zone peaks at 1000 km, which indicates a substantial increase in the bottom loss suffered by the RSR modes at this range. For the 244-meter SUS, this oceanographic feature is marked by the sudden appearance of convergence zones. Effects similar to these have been observed during a previous propagation trial in the same area (Ref. 19).

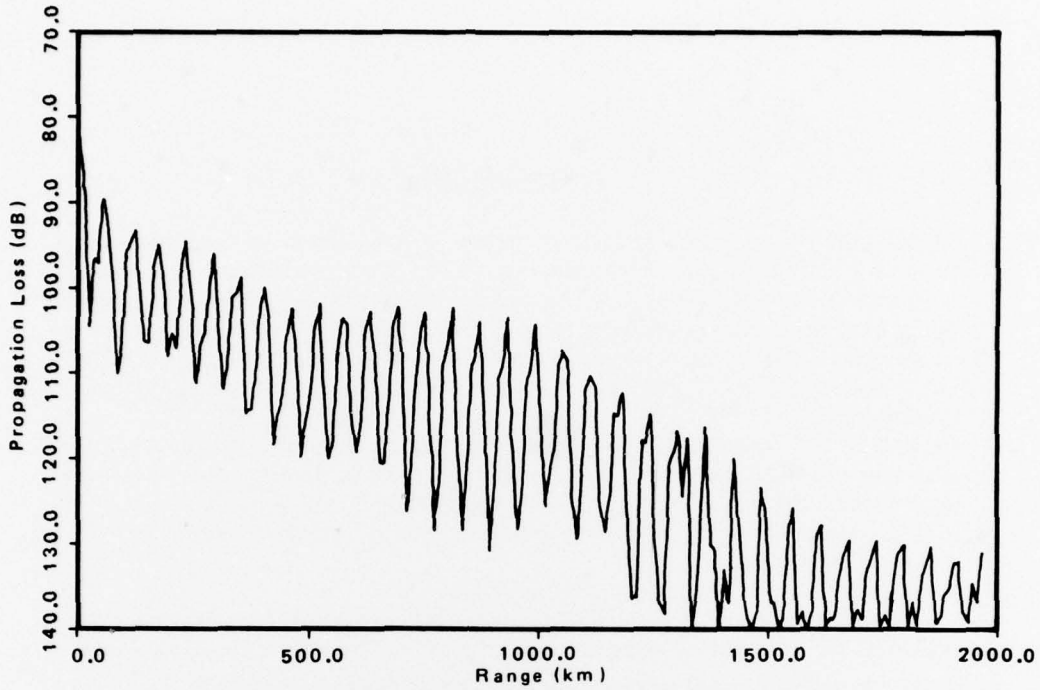

Figure 22. Radial NW: Parabolic equation propagation loss prediction for 18-meter SUS, 63 Hz frequency.

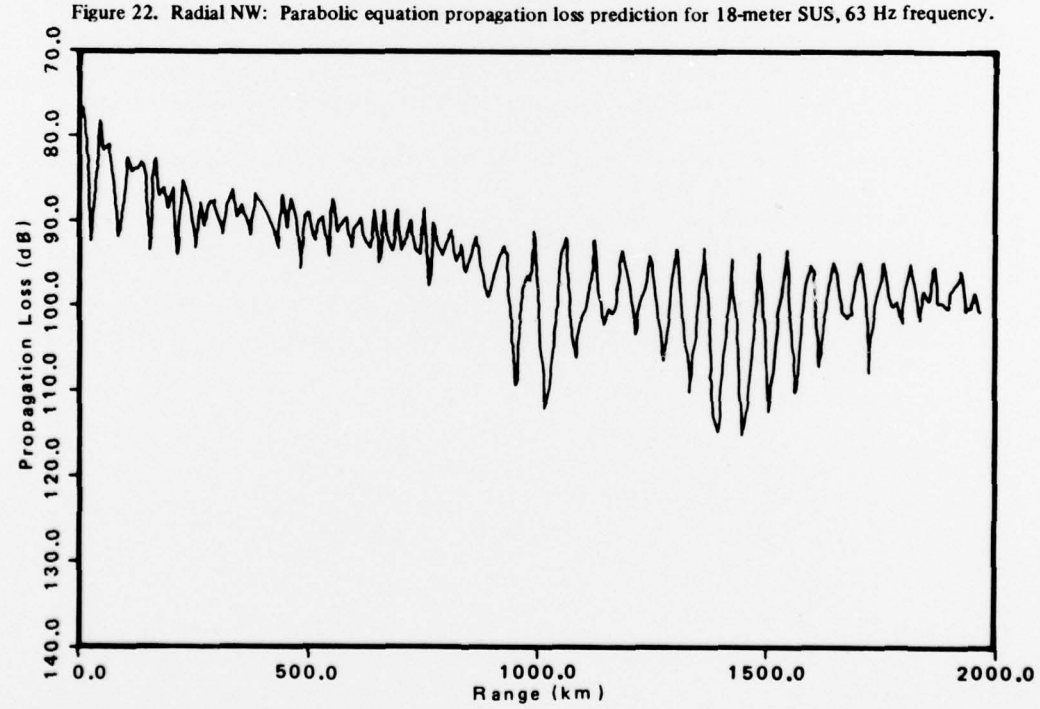

Figure 23. Radial NW: Parabolic equation propagation loss predication for 244-meter SUS, 63 Hz frequency.

CONCLUSIONS

We have used a parabolic equation model to study acoustic propagation over a wide variety of typical ocean environments. Bathymetric conditions encountered have included continental slopes, ocean basins, underwater ridges, and seamounts. In addition, the oceanographic conditions have varied from those typical of subtropical waters in the north to antarctic waters south of the Polar Front. These conditions have presented a severe test of the capabilities of current acoustic modeling techniques.

In spite of difficulties both in initializing and in running the parabolic equation model on the continental slope, the general level of agreement between measurement and prediction is encouraging. On a detailed scale, many aspects of the prediction are unsatisfactory, but there are several avenues worth exploring which may improve the agreement.

Key conclusions resulting from this work are:

1. In environments where the water depth may change substantially, such as near continental slopes or underwater features, and in regions where the water depth is marginal for RSR propagation, considerable care needs to be exercised in the choice of vertical sample size, Δz, to ensure that the highest order modes needed are sampled properly at all ranges. To proceed efficiently and to minimize computer running costs, the model should automatically adjust Δz to suit the local conditions.

2. Small changes in sound-speed profile may induce operationally significant changes in acoustic propagation characteristics.

3. Acoustic shadowing behind substantial underwater features is strongly dependent on the nature of the sediment cover.

4. The knowledge of gross sound-speed characteristics and sea floor properties alone may not be sufficient to model acoustic propagation characteristics in all ocean regions. For example, there may be energy loss as a result of mode coupling either from surface roughness where there is no deep sound channel, or from inhomogeneities within the water column in the boundry region between different water mass types.

Appendix

APPLICABILITY OF SMALL-ANGLE APPROXIMATION

Here consider the "small-angle" approximation used to derive the parabolic equation (Eq. 6). This is usually expressed by the requirement that

$$\left| \frac{\partial^2 U}{\partial r^2} / 2ik_0 \frac{\partial U}{\partial r} \right| \ll 1 \tag{8}$$

To demonstrate that this condition is valid in the deep sound channel, we consider the expression for the propagation of a normal mode under the parabolic equation approximation. Comparing Eq. 5 and 10, we obtain the following expression for U:

$$U(r,z) \approx U_m(z) \exp(K_m^2 r / 2ik_0) \tag{A-1}$$

Differentiating (A-1) with respect to r twice we have

$$\frac{\partial^2 U}{\partial r^2} \approx \left(\frac{K_m^2}{2ik_0} \right) \frac{\partial U}{\partial r} \tag{A-2}$$

Substituting this last equation into Eq. 8, the condition to be satisfied is:

$$\frac{K_m^2}{4k_0^2} = \left(\frac{\sin\theta_0}{2} \right)^2 \ll 1 \tag{A-3}$$

where we have used the well-known (Ref. 13) definition of equivalent ray angle, θ_0, to simplify the expression.

Maximum values of θ_0 usually significant in a deep ocean sound channel are typically 0.3 radian. Thus, for this type of propagation the small-angle approximation is easily satisfied.

REFERENCES

1. R.W. Bannister et al., "Project Tasman Two: low frequency propagation measurements in the South Tasman Sea," J. Acoust. Soc. Amer., Vol 58, 1975, S85.
2. F.D. Tappert, "Parabolic equation method in underwater acoustics," J. Acoust. Soc. Amer., Vol.55, 1974, S34
3. K.M.Guthrie, "Collated environmental data for Tasman Two," DSE Misc. 75 /7, September 1975.
4. A.L. Gordon, "Introduction: physical oceanography of the Southeast Indian Ocean" in Antarctic Oceanology II: The Australian - New Zealand Sector, Antarctic Res. Serv. Vol.19, edited by D.E. Hayes, AGU, Washington, D.C. 1972, pp 3 - 9.
5. D.E. Hayes, "Introduction: marine geophysics of the Southeast Indian Ocean" in Antarctic Oceanology II: The Australian - New Zealand Sector, Antarctic Res. Ser. Vol.19 edited by D.E. Hayes, A.G.U. Washington, D.D. 1972,pp 119 - 124.
6. R.J. Urick, "Handy curves for finding the source level of an explosive charge fired at depth in the sea," J. Acoust. Soc. Amer., Vol.49, 1971, pp 935 - 936.
7. "NAVSEA ocean environmental acoustic data bank - NAVDAB - in support of mobile sonar technology development," Vol 1 - 5, Report No. SEA 06H1/036-EBA/MOST-3, 1975
8. J.B. Kennett et al., "Initial reports of Deep Sea Drilling Project," Vol. XXIX, U.S. Government Printing Office, Washington, D.C. 1975.
9. R.E. Houtz, "Comparison of sonobuoy and sonic probe measurements with drilling results," in Ref. 8, pp 1123 - 1131.

10. R.E. Houtz, "South Tasman Basin and Borderlands: a geophysical summary," in Ref. 8, pp 1135 - 1146.

11. E.L. Hamilton, "Sound attenuation in marine sediments," NUC TP 281, 1972.

12. F. Jensen, H. Krol, "The use of the parabolic equation method in sound propagation modelling," SACLANTCEN Memorandum SM-72, August 1975.

13. J. Tolstoy, C.S. Clay, "Ocean acoustics," McGraw-Hill, New York, 1966.

14. D.M. Milder, "Ray and wave invariants for SOFAR channel propagation," J. Acoust. Soc. Amer., Vol. 46, 1969, pp 1259 - 1263.

15. W.G. Kanabis, "A shallow water acoustic model for an ocean stratified in range and depth," Vol. 1, NUSC Technical Report 4887-I 1975.

16. R.D. Graves et al., "Range-dependent normal modes in underwater sound propagation: application to the wedge-shaped ocean," J. Acoust. Soc. Amer., Vol. 58, 1975, pp 1171 - 1177.

17. R.M. Fitzgerald, "Helmholtz equation as an initial value problem with application to acoustic propagation," J. Acoust. Soc. Amer., Vol. 59, 1975, pp 839 - 842.

18. S.T. McDaniel, "Propagation of a normal mode in the parabolic approximation," J. Acoust. Soc. Amer., Vol. 57 1975, pp 307 - 311.

19. A.C. Kibblewhite, R.N. Denham, "Long-range sound propagation in the South Tasman Sea," J. Acoust. Soc. Amer., Vol. 41, 1967, pp 401 - 411.